

# Application of Electric Current-Assisted Sintering Techniques for the Processing of Advanced Materials

Martin Bram,\* Alexander M. Laptev, Tarini Prasad Mishra, Kushnuda Nur, Moritz Kindelmann, Martin Ihrig, Joao Gustavo Pereira da Silva, Ralf Steinert, Hans Peter Buchkremer, Andrey Litnovsky, Felix Klein, Jesus Gonzalez-Julian, and Olivier Guillon

Highly efficient energy conversion and storage technologies such as high-temperature solid oxide fuel and electrolysis cells, all-solid-state batteries, gas separation membranes, and thermal barrier coatings for advanced turbine systems depend on advanced materials. In all cases, processing of ceramics and metals starting from powders plays a key role and is often a challenging task. Depending on their composition, such powder materials often require high sintering temperatures and show an inherent risk of abnormal grain growth, evaporation, chemical reaction, or decomposition, especially in the case of long dwelling times. Electric current-assisted sintering (ECAS) techniques are promising to overcome these restrictions, but a lot of fundamental and practical challenges must be solved properly to take full advantage of these techniques. A broad and long-term expertise in the field of ECAS techniques and comprehensive facilities including conventional field-assisted sintering technology/spark plasma sintering (FAST/SPS), hybrid FAST/SPS (with additional heater), sinter forging, and flash sintering (FS) devices are available at the Institute of Energy and Climate Research: Materials Synthesis and Processing (IEK-1). Herein, main advantages and challenges of these techniques are discussed and the concept to overcome current limitations is introduced on selected examples.

## 1. Introduction


Electric and magnetic fields provide an additional degree of freedom to synthesize, process, and tune the microstructure of inorganic materials.<sup>[1]</sup> Electric current-assisted sintering (ECAS) techniques are highly promising for the processing of advanced materials due to significant enhancement and acceleration of sintering kinetics compared with conventional sintering technologies.<sup>[2–7]</sup> Starting from first patents more than 100 years ago, today more than 50 different principles of ECAS techniques are described in patents and literature.<sup>[3]</sup> In general, short-term sintering with high heating rates and low dwell times can be achieved by 1) indirect heating of nonconductive powders in a conductive tool, which is heated by the Joule effect and conducts the heat to the powder; 2) indirect heating of nonconductive powders by induction or thermal radiation up to an onset temperature, where current starts to flow through

the sample and therefore direct heating becomes possible; 3) direct heating of conductive powders by the Joule effect directly dissipating energy within the sample; and 4) ultrafast direct heating of conductive powders by sudden release of energy stored in a capacitor via the sample. Electrical conductivity of the powder and tool material mainly decides if sample is heated directly or indirectly. Metals, alloys, and specific ceramic materials like TiC, TiN, Ti(C,N), MAX-phases (M = transition metal, A = A group element, and X = C or N), WC, TiB<sub>2</sub>, and ZrB<sub>2</sub> as ultrahigh temperature ceramics (UHTCs) can be directly heated in field-assisted sintering technology/spark plasma sintering (FAST/SPS) mode as their electrical conductivities are orders of magnitude higher than electrical conductivity of graphite, usually applied as tool material. *Visa versa*, most oxides (Al<sub>2</sub>O<sub>3</sub>, ZrO<sub>2</sub>, YSZ, MgO, CeO<sub>2</sub>, gadolinium-doped ceria [GDC], etc.) and other ceramics like BN, Si<sub>3</sub>N<sub>4</sub>, SiC, and B<sub>4</sub>C are indirectly heated due to their low electrical conductivity. The efficiency of ECAS techniques can be further increased by applying uniaxial pressure, which additionally supports the sintering kinetics, therefore enabling to lower the sintering temperature

Dr. M. Bram, Prof. A. M. Laptev, T. P. Mishra, K. Nur, M. Kindelmann, M. Ihrig, Dr. J. G. Pereira da Silva, R. Steinert, Dr. H. P. Buchkremer, Prof. A. Litnovsky, Dr. F. Klein, Prof. J. Gonzalez-Julian, Prof. O. Guillon  
Institute of Energy and Climate Research (IEK)

Forschungszentrum Jülich GmbH  
52425 Jülich, Germany  
E-mail: m.bram@fz-juelich.de

Prof. O. Guillon  
JARA-Energy  
Jülich Aachen Research Alliance  
52425 Jülich, 52066 Aachen, Germany

 The ORCID identification number(s) for the author(s) of this article can be found under <https://doi.org/10.1002/adem.202000051>.

© 2020 The Authors. Published by WILEY-VCH Verlag GmbH & Co. KGaA, Weinheim. This is an open access article under the terms of the Creative Commons Attribution-NonCommercial-NoDerivs License, which permits use and distribution in any medium, provided the original work is properly cited, the use is non-commercial and no modifications or adaptations are made.

DOI: 10.1002/adem.202000051

and time. ECAS techniques offer several advantages, which are difficult to achieve with established sintering techniques. In the case of materials, where the activation energy of sintering is higher than the activation energy of grain growth, high heating rates (usually in the range of  $10^2$ – $10^6$  K min<sup>-1</sup>) can be advantageously used to reliably limit or even inhibit grain growth and therefore maintain fine-grained microstructures. Therefore, tailoring of microstructures down to the nanometer scale becomes possible. Furthermore, chemical reactions, decomposition, or evaporation of thermodynamically less-stable materials can be significantly reduced or completely avoided. ECAS techniques are often the preferred method to produce dense parts from materials which are difficult to sinter with conventional methods. Examples are refractory materials like borides, nitrides, and carbides, complex alloyed materials like compounds for electrochemical devices, or composite materials combining phases with large difference of properties like diamond-reinforced tool steels.<sup>[8]</sup> Finally, ECAS techniques promise reduction of overall energy consumption, especially if effective heat transfer and short cycle times are combined. Challenges of ECAS technologies are limitations regarding net shaping of complex geometries, choice of the right tool material, and suitable interface design. Three specific ECAS technologies are shortly introduced in the following paragraphs due to their relevance to this work.

### 1.1. Field-Assisted Sintering Technology/Spark Plasma Sintering

FAST/SPS devices consist of a conductive tool, which is placed between two water-cooled metallic electrodes.<sup>[9,10]</sup> The setup is placed in a water-cooled chamber, which enables operation of the device in vacuum or protective atmosphere (e.g., Ar, Ar/H<sub>2</sub>, N<sub>2</sub>). For heating, moderate voltages below 10 V and high currents up to several 1000 A are applied to the tool via the electrodes. Usually, FAST/SPS devices are operated with direct current (DC). Optionally, current can be pulsed with pulse durations ranging from milliseconds to seconds. Based on power source and sample geometry, heating rates up to 1000 K min<sup>-1</sup> become possible. High heating rates are the basis for clearly reducing cycle time compared with conventional sintering. To keep the contact resistance at the tool–powder interface low, a conductive interlayer (e.g., graphite foil) is usually introduced, which also avoids sticking of the material on the tool walls. In standard configuration, water cooling of electrodes enables cooling rates up to 150 K min<sup>-1</sup>, but the maximum rate is strongly influenced by tool design and optional application of thermal insulation covering the die wall (e.g., graphite felt). Such insulation can be advantageous with respect to decreasing heat loss by thermal radiation, therefore reducing thermal gradients, thermally induced stresses, and energy consumption.<sup>[11]</sup> If aiming on cooling rates higher than 150 K min<sup>-1</sup>, the device must be equipped with active cooling, e.g., by controlled gas flow. A hydraulic system enables applying a controlled pressure during the sintering cycle, which is mainly affected by the tool material, the construction of the device, and the diameter of the pressing tool. If graphite is used as the tool material, pressures in the range of 50–100 MPa are usually applied. Special qualities of graphite enable pressures up to 230 MPa.<sup>[12]</sup> If graphite tools



**Martin Bram** studied materials science at the University Erlangen-Nürnberg and received his diploma degree in 1995. He got his Ph.D. degree in materials science in 1998 from University of Saarland, Saarbrücken. Currently, he is working as a group leader in the field of “Powder based processing and sintering” at the Institute of Energy and Climate Research (IEK-1: Materials Synthesis and Processing) of Forschungszentrum Jülich GmbH. In 2012, he completed his habilitation from Ruhr University Bochum. His main research interests are powder-based processing and sintering of materials for energy applications such as metal-supported fuel cells, electrolyzers, batteries, and high temperature materials.



**Olivier Guillon**, following an engineering degree at the Alès School of Mines, completed his Ph.D. on ferroelectric ceramics. After post-docs at University Darmstadt and University of Washington, he established a DFG funded Emmy Noether Group on new ceramic processes. After a first professorship from the University of Jena, he became Director at the Institute of Energy and Climate Research – Materials Synthesis and Processing (Forschungszentrum Jülich) and professor at the RWTH Aachen University in 2014. His research interests are science and technology of sintering, ceramic barrier coatings and ceramic matrix composites, solid oxide fuel/electrolysis cells, gas separation membranes and solid-state batteries.

are used, maximum temperatures up to 2400 °C are possible. Alternative tool materials enable significantly higher pressures up to the GPa range, but then restrictions regarding the maximum temperature come into play, which will be discussed in more detail later. Exact measurement of the sample temperature is a challenging task in FAST/SPS setups. Uncertainty of temperature measurement can lead to conflicting results. Usually, temperature measurement is carried out either by thermocouple(s) or pyrometer(s). In both cases, temperature of the punch or the die wall is measured at distinct positions. To reduce the distance to the sample, normally holes are drilled at these positions. At temperatures below 1100 °C, a K-type thermocouple can be applied. To overcome uncertainties of temperature measurement, predictive methods like finite element modeling (FEM) of temperature distribution are frequently used for optimization of FAST/SPS tool design and sintering parameters.<sup>[13]</sup> Densification of powders in FAST/SPS devices is characterized by a superposition of mechanical, thermal, and current effects. In addition to Joule heating, Peltier effect and electrochemical reactions at the tool–sample interface might influence densification and grain growth. In the case of conductive samples, thermal and current effects cannot be ambiguously separated. A more

detailed summary of densification mechanisms in FAST/SPS device can be found in the literature.<sup>[8,10,14]</sup> As interesting alternative, hybrid FAST/SPS, was introduced recently, which combines FAST/SPS with other heating methods like induction or resistance heating, aiming to further increase heating rates and thermal homogeneity<sup>[15]</sup> or the opposite, to create temperature gradients on purpose. For high-throughput manufacturing, industrial hybrid sintering plants with additional preheating and cooling channels are under development as well.<sup>[15]</sup>

## 1.2. Application of FAST/SPS for Synthesis of High-Performing Materials

As mentioned earlier, the application of electric field and mechanical load in FAST/SPS devices provides the additional degree of freedom to synthesize high-performing materials. The instrumentation of present-day FAST/SPS devices enables to control field- and pressure-assisted sintering cycles with high accuracy. Based on this, FAST/SPS became a powerful tool for target-oriented development of new material systems with tailored microstructures.<sup>[9]</sup> Recently, FAST/SPS has been successfully applied, e.g., for the development of all-solid-state-battery materials,<sup>[16,17]</sup> UHTCs,<sup>[18]</sup> transparent ceramics,<sup>[19,20]</sup> high entropy alloys,<sup>[21]</sup> as well as thermoelectric and magnetic materials.<sup>[22]</sup> Another important area of application is manufacturing of high-performing lightweight alloys based on Al,<sup>[23]</sup> Mg,<sup>[24,25]</sup> or titanium,<sup>[26]</sup> e.g., by controlled crystallization of amorphous starting powders in a FAST/SPS device.<sup>[27,28]</sup> This approach is especially attractive for high strength structural<sup>[28]</sup> and—in the case of titanium alloys—for biomedical applications.<sup>[29]</sup> From a scientific point of view, the highly accurate control of all process parameters enables to study densification mechanisms in the presence of electric fields<sup>[30–34]</sup> and identify main processing factors required for tuning grain boundaries,<sup>[35,36]</sup> texture,<sup>[37]</sup> porosity,<sup>[38]</sup> and other functional properties. For a more detailed discussion of the big potential of FAST/SPS techniques for material synthesis and microstructure tuning, we refer to excellent textbooks summarizing the current state of the art.<sup>[6–8]</sup>

## 1.3. Flash Spark Plasma Sintering

Flash spark plasma sintering (FSPS) is a novel operation mode, which can be conducted in conventional FAST/SPS devices. FSPS has been demonstrated for the first time by Grasso et al.<sup>[39]</sup> and requires specific tool design to enable preheating of the sample before onset of current flow. Alternatively, induction or radiation heating as available in hybrid FAST/SPS devices can be used for this purpose.<sup>[40–42]</sup> FSPS is characterized by the low voltage of maximum 10 V and very high heating rates in the range of  $10^4$ – $10^6$  K min<sup>−1</sup>.<sup>[43]</sup> Furthermore, densification is supported by applying a well-defined mechanical load. Rapid heating is achieved by a DC current pulse with a defined length enabling sudden supply of extremely high heating power. To avoid overheating and sample melting, operation of the FAST/SPS device is done by limiting the maximum power during the current pulse. After achieving the maximum power, the sample is discharged by holding this power for several seconds and rapidly densifying.

The estimation of temperature distribution during the flash event by numerical simulation indicates the occurrence of large temperature gradients up to several 100 °C,<sup>[40]</sup> which is critical if aiming to achieve homogeneous microstructures.

FSPS does not have the same flexibility regarding the choice of materials and adjustment of parameters like FAST/SPS, but it has the potential to transfer ultrarapid densification concepts like electrodischarge sintering (EDS)<sup>[44,45]</sup> and electroresistance sintering (ERS)<sup>[46]</sup> to FAST/SPS devices. While these technologies are limited to electrically conductive materials, FSPS has been successfully applied to nonoxide ceramics like B<sub>4</sub>C and SiC,<sup>[39,40,47–49]</sup> which were—despite their high melting points—successfully densified to almost theoretical density within seconds. Grasso et al. reported the manufacturing of a crack-free SiC sample with a diameter of 60 mm.<sup>[40]</sup> FEM simulation of the sample temperature reveals temperature gradients in the range of 200–300 °C between the core and the surface and risk of hot spot formation as the main challenges of FSPS technology.<sup>[40,48]</sup> Vasylykiv et al.<sup>[50]</sup> and Manière et al.<sup>[43]</sup> even successfully applied FSPS for the densification of oxide ceramics (i.e., 3YSZ or Al<sub>2</sub>O<sub>3</sub>). Scanning electron microscopy (SEM) investigations revealed that the initial crystallite size of the starting powder was retained in the sintered sample.

## 1.4. Flash Sintering

Flash sintering (FS) is an attractive alternative to the sintering methods discussed earlier. FS was discovered by Raj and coworkers<sup>[51]</sup> and has been successfully applied for a large number of ceramic materials.<sup>[52]</sup> For initiating FS, a current is forced within a ceramic body by applying an electric field in combination with external heating. Contrary to FSPS, much higher electric fields up to several 100 V cm<sup>−1</sup> are used, whereas current densities during the flash event remain in the range of a few A cm<sup>−2</sup>. When exceeding a specific onset temperature, the sample becomes sufficiently conductive, and electric current starts suddenly to pass through the sample. This avalanche-like effect is accompanied by luminescence and very fast densification in few seconds. As the heating power is almost completely dissipated by the sample, FS is discussed to be a very energy-efficient and economic process,<sup>[52,53]</sup> and the development of large-scale FS kiln by the UK company Lucideon was reported recently.<sup>[54]</sup> Mechanisms of FS are still under debate. Proposed mechanisms are thermal runaway, internally generated by Joule heating,<sup>[55,56]</sup> grain boundary overheating with local melting,<sup>[57,58]</sup> extremely high heating rates,<sup>[49,59]</sup> modification of grain boundaries leading to accelerated diffusion,<sup>[60,61]</sup> formation of defects like Frenkel pairs,<sup>[62,63]</sup> or oxygen vacancies in the case of oxides. The latter ones are indicated by electrochemical blackening.<sup>[64]</sup> It has been recently shown that even below the FS threshold, enhanced sintering stress and lower viscosities are obtained while maintaining a constant sample temperature, showing the clear athermal effect of electric field loading.<sup>[60]</sup>

## 1.5. Aim of This Work

ECAS techniques are in multiple use for sample preparation on a laboratory scale and gained a lot of interest in the scientific

community within the past decade, aiming at understanding how electric fields and current flow influence the sintering mechanisms of ceramics and metals. However, only FAST/SPS has been successfully transferred to industrial production, but it is still a niche market. Still numerous open fundamental and practical questions remain, which are rarely discussed in the literature but must be reliably answered to establish and take full advantage of ECAS techniques. In this context, the following challenges are addressed: 1) Developing strategies to sinter materials which are prone to evaporation, chemical expansion, and decomposition, especially under reducing conditions usually being existent in conventional FAST/SPS setups. 2) Taking advantage of alternative tool materials to increase the maximum pressure. 3) Developing strategies to sinter high-temperature and refractory materials. 4) Developing strategies to do net shaping in FAST/SPS devices. 5) Reducing temperature gradients to a minimum to avoid density gradients and residual stresses, e.g., by thermal insulation or hybrid heating. 6) Scaling up of the technology while maintaining homogeneous microstructures. 7) Reducing the overall energy demand to a minimum. 8) Combining FAST/SPS and FS technologies.

In this work, our strategies to work on these challenges of ECAS techniques are introduced. Therefore, related experiments were conducted on specific ceramic and metallic materials belonging to the portfolio of the institute, and examples of application are discussed with respect to literature. All experiments were done on a conventional, lab-scale FAST/SPS device (HP-D5, FCT Systeme GmbH, Germany) and on a unique equipped hybrid FAST/SPS device (H-HP-D25 SD/FL/MoSi, FCT Systeme GmbH, Germany), which enables operation in the conventional FAST/SPS mode, hybrid FAST/SPS mode with an additional heater, and FSPS mode. Furthermore, the device is uniquely equipped with a 1000 V alternating current (AC) and DC power sources, which are expected to enable FS of larger-scaled pellets or plates.

## 2. Equipment and Methods

In this section, sintering facilities, specific tool materials, and strategies to predict temperature distribution by FEM are introduced. Starting materials used for our experiments will be described in Section 3. For other experimental details like temperature measurement or material characterization methods, we refer to the cited literature.

### 2.1. Sintering Facilities

Three FAST/SPS devices are operated at IEK-1. On a lab scale, HP-D5 device from FCT Systeme GmbH, Rauenstein, Germany, enables to sinter samples with a diameter of maximum 30 mm and a maximum height of 50 mm. A power source of 37 kW enables to achieve maximum temperature of up to 2400 °C at a maximum voltage of 8 V. Under standard conditions, a pulsed DC with 25 ms current and 5 ms pause is used. The mechanical load can be varied between 2 and 50 kN. In comparison with standard machines, the minimum applicable mechanical load has been reduced significantly to be able to densify green bodies processed separately.<sup>[65]</sup> The device is equipped with a gas-tight

chamber, which enables gas pressures in the range of  $10^{-2}$ –1000 mbar. The system can be operated in moderate vacuum ( $\approx 0.5$  mbar) as well as with protective gases Ar, Ar/2.9% H<sub>2</sub>, and N<sub>2</sub>. Furthermore, technical air can be also used by the connection of working chamber with a gas bottle or gas supply system. However, the use of technical air must be performed with caution because it can react with tool or powder material at a high temperature. For instance, graphite intensively starts to burn out in air at 600 °C.

On a larger scale, H-HP-D25 SD/FL/MoSi device also from FCT Systeme GmbH is constructed as hybrid FAST/SPS with an additional heater and can be operated in the FS mode as well. In summary, the device enables four modes of operation: 1) conventional FAST/SPS, 2) hybrid FAST/SPS with an additional heater, 3) FS with an AC/DC power source and additional heater, and 4) hot press with radiation heating. The maximum sample size is  $100 \times 100 \text{ mm}^2$  and the maximum sample height is  $\approx 50$  mm. The heating power is 60 kW for FAST/SPS heating at maximum 8 V and 80 kW for additional hybrid heating, which can be done by an induction coil or a MoSi<sub>2</sub> heater. As a further option, a 1000 V voltage source enables FS of powder compacts. The power source delivers DC or AC, the latter with a frequency in the range of 10 Hz–80 kHz. For FS, the samples are contacted by two Pt electrodes, which are placed between the punches. In the FS mode, the high-power electrical circuit of the FAST/SPS mode has to be turned off. The process gas chamber enables operation in moderate vacuum ( $\approx 0.5$  mbar) and with Ar, Ar/2.9% H<sub>2</sub>, N<sub>2</sub>, and technical air.

For further scaling up of technology, FAST/SPS device DSP 515 from Dr. Fritsch, Fellbach, Germany, enables sample sizes up to  $180 \times 180 \text{ mm}^2$  and a maximum height of  $\approx 60$  mm. The heating power is 170 kW, and the mechanical load can be varied between 47 and 555 kN. The device is equipped with a process gas chamber, which enables a vacuum of 20 mbar and an in situ debinding of organic-containing specimens. Furthermore, Ar, Ar/2.9% H<sub>2</sub>, N<sub>2</sub> atmospheres, and technical air are possible atmospheres.

### 2.2. Tool Materials

#### 2.2.1. Graphite Tools and Graphite-Based Setup Components

All graphite materials used in this work were delivered by SGL Carbon GmbH, Germany. For manufacturing of graphite tools, fine-grained SIGRAFINE R7710 graphite was used. To improve the contact between punch and sample as well as between punch and die, SIGRAFEX graphite foil, grade E, was used, which is available in different thicknesses (e.g., 0.35 mm). To improve thermal insulation of the die, SIGRATHERM soft graphite felt, grade GFA 10 with a thickness of 11.5 mm, was applied. Finally, to reduce the heat loss via the water-cooled electrodes, carbon fiber-reinforced carbon (CFRC) spacers were conducted from SIGRABOND Premium CFRC composite. CFRC had almost the same electrical resistivity like graphite but a significantly lower thermal conductivity.<sup>[11]</sup> For estimating the current and temperature distribution, anisotropic properties of the graphite foil have to be considered. The foil has a higher electrical resistivity than bulk graphite, which furthermore differs in vertical ( $1\text{--}10 \text{ } \Omega \text{ mm}$ ) and horizontal direction ( $0.1\text{--}3 \text{ } \Omega \text{ mm}$ ).

Specific graphite tool design used in our experiments is described in more detail in Section 3.

### 2.2.2. Steel Tools

Despite graphite being an excellent tool material for high temperature sintering, its strength is relatively low. As an upper limit, a compressive strength of 230 MPa is reported in the literature for an isostatically pressed graphite, which has been especially developed for FAST/SPS applications.<sup>[12]</sup> High strength is achieved by a very small grain size ( $\approx 5 \mu\text{m}$ ). Nevertheless, such graphite qualities are often too expensive for industrial application. In general, all grades of graphite are brittle and prone to mechanical wear. In FAST/SPS practice, loading of graphite with a maximum pressure of 50 MPa is recommended for long-term use of tools. This value also considers the tensile mode of loading for the graphite die.

To broaden the range of applications of FAST/SPS, increase in pressure can be beneficial to achieve the required density at a lower temperature. Reduced sintering temperature retards grain growth, results in fine-grained microstructure, decreases energy consumption, and in some cases allows to avoid undesirable reactions and decomposition of sintered materials. To apply higher pressures, tool materials other than graphite must be used. In particular, steel tools are attractive alternatives to graphite tools. Of course, application of steel tools is limited to a certain temperature range. We successfully introduced steel tools made of hot working steel grade W-360 (Böhler, Germany) for cold sintering of ZnO ceramics, applying pressure of up to 300 MPa and temperatures in the range between 250 and 400 °C (Section 3.1). The tool has held out many cycles without any visible damage or wear. Based on properties reported by Böhler,<sup>[66]</sup> the application of FAST/SPS tool manufactured from this kind of steel seems to be reasonable up to 600 °C, but further work is required to prove this assumption.

### 2.2.3. TZM Tools

Another option for replacement of graphite as a tool material is application of molybdenum-based Ti–Zr–Mo (TZM) alloy (Plansee, Austria<sup>[67]</sup>). TZM was developed as a material for high-temperature application in particular for forging tools. Plansee reports possible application temperatures in the range of 700–1400 °C. However, the yield strength of TZM is clearly reduced if application temperature exceeds 1100 °C. Another concern in high-temperature application of TZM is the risk of recrystallization accompanied by significant decrease in strength and ductility. Although recrystallization temperature of TZM ( $\approx 1100$  °C) is larger than that for pure molybdenum, a possible local overheating can lead to failure of the tool. Therefore, we restrict application temperature of our TZM tools to 1100 °C at a maximum pressure of 350 MPa. At a lower temperature, the applied pressure can be increased, but possible creep of material must be carefully considered. In this work, TZM tools were used for sintering of NASICON samples at 700 °C and 300 MPa<sup>[68]</sup> and for LLZ/LiCoO<sub>2</sub> (LCO) all-solid-state battery half cells at 675 °C and 440 MPa.<sup>[69]</sup> For more details, see Section 3.2.

## 2.3. Modeling of Temperature Distribution

Temperature distribution is an important issue in FAST/SPS technology and related tool design. During FAST/SPS cycles, the temperature can be recorded at several points, but only one measurement is used for control of supplied power. Moreover, the temperature inside the compacting powder cannot be measured at all. In contrast, the temperature distribution can be quite inhomogeneous.<sup>[13,70]</sup> A classic misinterpretation is to define the temperature measured on the thermal noninsulated die wall as the sintering temperature of the sample. Zavaliangos and coworkers<sup>[70]</sup> showed that these temperatures can differ up to several hundred degrees in the worst case. This mistake can lead to underestimation of temperature inside the sample and incorrect temperature control. Even if temperature is measured in the vicinity of sample center, e.g., by drilling a hole in the upper punch of the FAST/SPS tool, this temperature can be still quite different from the temperature at the sample edge.<sup>[11]</sup> If temperature gradients exceed a critical value, inhomogeneity in densification, microstructure, and properties of the sintered sample results.<sup>[71]</sup>

To avoid such problems, FEM of temperature distribution inside both the sample and FAST/SPS tool is required. If done in an appropriate way, FEM allows: 1) understanding of temperature field in the whole experimental setup, 2) optimization of tool design aiming to reduce temperature gradients, and 3) evaluation of the required power and estimation of energy consumption depending on the specific setup construction. FAST/SPS modeling is usually discussed as a coupled thermo-electric-mechanical problem. Software possessing-related capabilities are required for such kind of modeling. Comsol, Abaqus, and Ansys are the mostly used software for FAST/SPS simulation. In particular, we use Ansys-based APDL code for this aim. In addition to this software, a database including the thermal, electric, and mechanical properties of sintered material and materials of setup elements is required. Moreover, all these properties must be available in whole range from ambient temperature to sintering temperature and as a function of density. Determination of such data is not a simple (and therefore time-consuming) task, especially in the case of new materials, powder composites, and materials with phase transition or reactively sintered materials. A collection of properties required for modeling of many materials is available at IEK-1. It is worth mentioning that the problem can be reduced to thermal–electric analysis if densification is completed. This situation is typically achieved at the end stage of sintering during dwell time. Then, only thermal and electric properties are needed for appropriate modeling. Usually, these data can be much more easily determined compared with mechanical properties. Therefore, a simplified thermal–electrical analysis is frequently used for modeling the whole FAST/SPS cycle.

In the work of Laptev et al.,<sup>[11]</sup> an example of FEM modeling of FAST/SPS cycles we conducted is given. Here, temperature distribution inside conductive (steel 316L) and nonconductive (8YSZ) samples of different sizes was analyzed. Large gradients were found especially in the case of 8YSZ samples with large diameters. As one of the main reasons, a nonoptimized setup design was discussed. Furthermore, the importance of the

careful thermal insulation for reduction of energy consumption and improvement of temperature homogeneity is highlighted. The use of geometry parameterization, link to materials' database, a built-in virtual PID controller, and an interactive input mode makes FAST/SPS modeling relatively easy to use and user friendly.

### 3. Examples of Application

In this section, a compact overview of current applications of ECAS technologies at Institute of Energy and Climate Research is given. As a broad spectrum of research topics is covered, it is not possible to give all experimental details in this work. For more details, we refer to the cited literature.

#### 3.1. Low-Temperature FAST/SPS of Oxide Ceramics by Applying Sintering Aids

Nanostructured polycrystalline materials are of interest for many applications due to expecting improved mechanical properties, enhanced wear resistance, and potential to tune functional properties like thermal or electrical conductivities. High density is desired for these kinds of applications as porosity usually affects physical properties. Among others, doping, extremely high pressures, and two-step sintering are methods which enable to retard grain coarsening if starting from nanosized powders. Another method to achieve this goal is adapting the idea of cold sintering to FAST/SPS technology (recently also named as Cool-SPS<sup>[72]</sup>). As described by several authors,<sup>[73,74]</sup> water-based sintering aids support of the densification of ceramic materials at very low sintering temperatures. By the combination of both technologies, advantages of FAST/SPS and cold sintering are combined, resulting in almost fully dense compacts with nanoscaled grains. Advantages of FAST/SPS are the better process control compared with the noninstrumented presses used for cold sintering currently in use.<sup>[75]</sup> Joule heating and direct heat transfer in a FAST/SPS tool enable to realize high heating rates, which is helpful to avoid premature evaporation of the sintering aid. Furthermore, if suitable tool materials are used high pressures can be applied, which strongly support the densification process. The use of water-based sintering aids in a FAST/SPS device may

have several benefits.<sup>[76,77]</sup> Water reduces die wall friction and friction between the particles leading to a better initial packing of the powder particles. Carbonates on the surface of powder particles, which might hinder the diffusion at the early sintering stage, are eliminated by being exchanged with water molecules. Depending on the material, water can trigger a solution-precipitation mechanism or at least—for smaller quantities of water—modify the diffusion mechanism. This mechanism can be further accelerated by enhancing the solubility of the material, e.g., by adapting the pH value accordingly. Dissociation of water can cause defect formation in the material, which might enhance densification by the formation of highly defective diffusion paths between the grains.

In the past years, we conducted comprehensive studies on nanosized ZnO.<sup>[76–79]</sup> ZnO with particle sizes below 100 nm was densified to almost theoretical density in our lab-scale FAST/SPS device HP-D5 at 250 °C by adding up to 3.2 wt% water to the powder compact. Use of steel tools enabled pressures up to 300 MPa. **Figure 1** shows the almost full densification of ZnO powder at these conditions, as an example. Densification at 250 °C proceeds up to a dwell time of 60 min with almost no grain growth. Due to the very high measured stress exponents (discarding pure liquid phase or diffusion-controlled densification), Gonzalez-Julian et al. proposed dislocation motion or grain boundary sliding as the possible superposed mechanisms.<sup>[77]</sup> To highlight the potential of cold sintering, sintering temperatures up to 900 °C are required to fully densify the same ZnO powders in a FAST/SPS device without addition of water. Here, oxygen diffusion along grain boundaries is discussed to be the rate-limiting mechanism of densification, and it is assumed that protons are accommodated in the lattice and grain boundaries, so that OH<sup>−</sup> ions become mobile instead of O<sup>2−</sup> ions.<sup>[76]</sup> Finally, it should be mentioned that the electric current is expected to play a negligible role during cold sintering of ZnO in a FAST/SPS device, as the electrical conductivity of ZnO at 250 °C is several orders lower than the conductivity of the steel tool.

Currently, the concept of cold sintering in a FAST/SPS device is transferred to materials for electrochemical devices. Pereira da Silva et al. investigated the potential of cold sintering for an all-solid-state-battery material. A solid electrolyte material with NASICON structure (Na<sub>3.4</sub>Sc<sub>0.4</sub>Zr<sub>1.6</sub>Si<sub>2</sub>PO<sub>12</sub>) showed an increased densification behavior at 250 °C, which could be

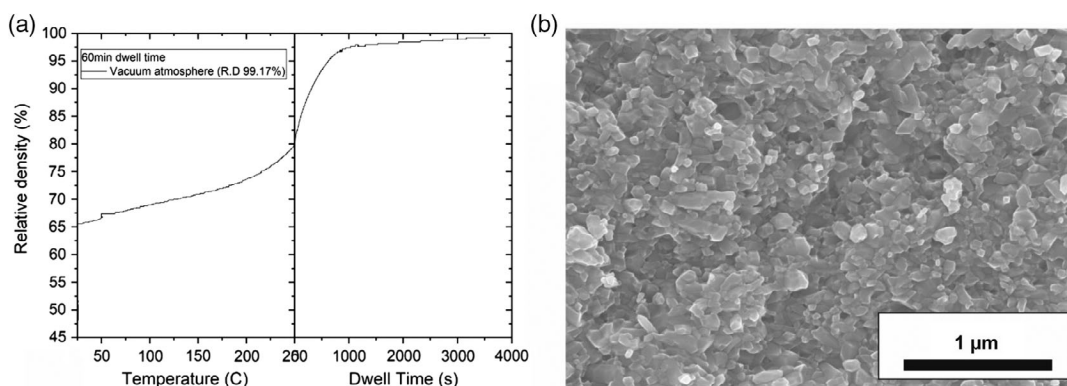


**Figure 1.** a) Densification of ZnO in a steel tool at 250 °C and 300 MPa by adding 3.2 wt% water to the powder compact. Almost full densification (99.17%) was achieved after a dwell time of 60 min. b) Maintaining the initial grain size of the starting powder in the cold sintered compact.

further improved by changing the pH value to strong acidic or basic conditions.<sup>[68]</sup> Another improvement in conductivity was achieved by a subsequent FAST/SPS treatment at 700 °C. Application of a Mo-based TZM tool enabled pressures up to 300 MPa, resulting in a sintering density >95%. Nevertheless, even at this high density, ionic conductivity of the NASICON electrolyte remained 1–2 orders of magnitude below the one of the related samples sintered by conventional FAST/SPS (1100 °C, 50 MPa) to the same density. This result hints on the fact that the physical properties are more influenced by the sintering process and the related constitution of the grain boundaries than by the final density. Further investigations are required to better understand the evolution of grain boundaries in the case of cold-sintered samples and their influence on the physical properties.

### 3.2. High-Pressure FAST/SPS of Materials Prone to Evaporation and Decomposition

The advantage of FAST/SPS to consolidate materials at low sintering temperatures, sintering with short dwell times, is especially crucial for energy materials showing a low thermal stability.<sup>[80,81]</sup> In case of one of the most promising oxide-based solid-state electrolyte  $\text{Li}_7\text{La}_3\text{Zr}_2\text{O}_{12}$  doped with Ta (LLZ:Ta), a sintering temperature well above the thermal stability of most cathode active materials for Li-ion batteries like  $\text{Li}[\text{Ni}_{1-x}\text{Co}_x\text{Mn}_y]\text{O}_2$  (NMC),  $\text{Li}[\text{Ni}_{1-x}\text{Al}_x\text{Mn}_y]\text{O}_2$  (NCA), and  $\text{Li}_2\text{NiMn}_3\text{O}_8$  (NMO) is required and carries out the preparation of composite cathodes without the usage of sintering additives difficult.<sup>[80,82–84]</sup> The standard cathode material LCO is compatible with cosintering with LLZ up to 1085 °C but contains the critical element Co and may form a high resistive interphase.<sup>[85]</sup> Other types of cathode materials massively react between 500 and 700 °C.<sup>[81]</sup> We recently developed a sintering method that allows to overcome these limitations. Cosintering of LLZ:Ta and LCO was successfully conducted by applying a high mechanical load (440 MPa) at moderate temperatures (675 °C) for short holding times in our lab-scale FAST/SPS HP-D5 device.<sup>[69]</sup> It is expected that this process is also applicable to less thermally stable active materials and hence offers the opportunity of novel material combinations for oxide-based composite cathodes based on NMC, NCA, and NMO.

However, FAST/SPS processing can also face new challenges for battery materials in comparison with conventional sintering: 1) The atmosphere in the process chamber can impact the thermal stability of the materials. 2) The contact between the materials and the graphite foil usually applied to improve the contact and protect the pressing tools results in reducing conditions, which might cause decomposition as well. Furthermore, carbon diffusion at the interface cannot be excluded reliably. 3) Surface impurities as especially found on LLZ like  $\text{Li}_2\text{CO}_3$  and LiOH might be stable at the used sintering temperature.<sup>[69,86,87]</sup>

Hence, a thorough optimization of the process parameters is vital to obtain improved properties of the sintered materials. 1) A promising approach to decrease the volatility of Li species, which further triggers material decomposition, was to switch the atmosphere from most generally used vacuum to Ar atmosphere.<sup>[69]</sup> 2) Side reactions, as for example the reaction of carbon with the LLZ:Ta-LCO mixture, are significantly reduced due to the short dwell time and low sintering temperature which also minimizes particle growth. The electrochemical properties of the powder material will therefore be conserved. 3) Surface impurities on LLZ:Ta are known to block ion conduction and are removed in conventional sintering due to high sintering temperatures.<sup>[86]</sup> Hence, the LLZ requires a clean surface which can be achieved by thermal removal before the FAST/SPS process.<sup>[88]</sup> In addition, applying high mechanical load up to 440 MPa was a helpful measure to obtain composite cathodes with more than 92% relative density (Figure 2a).<sup>[69]</sup>

Electrochemical proof of function of the composite cathode was achieved by the addition of a LLZ:Ta electrolyte on one side and subsequently attaching a Li-In anode on the other side, as described by Tsai et al.<sup>[85]</sup> The composite cathode could be discharged at an elevated temperature and showed an increased capacity compared with pure LCO cathodes (pure LCO cathode: 0.05 mA h cm<sup>-2</sup>, Figure 2b).<sup>[89]</sup>

### 3.3. Controlled Atmosphere FAST/SPS of Oxide Ceramics Prone to Chemical Expansion

Sintering of oxides in a FAST/SPS device can be a challenging task, especially in the case of materials like ceria or titanates, which tend to easily form oxygen vacancies in contact with graphite tools

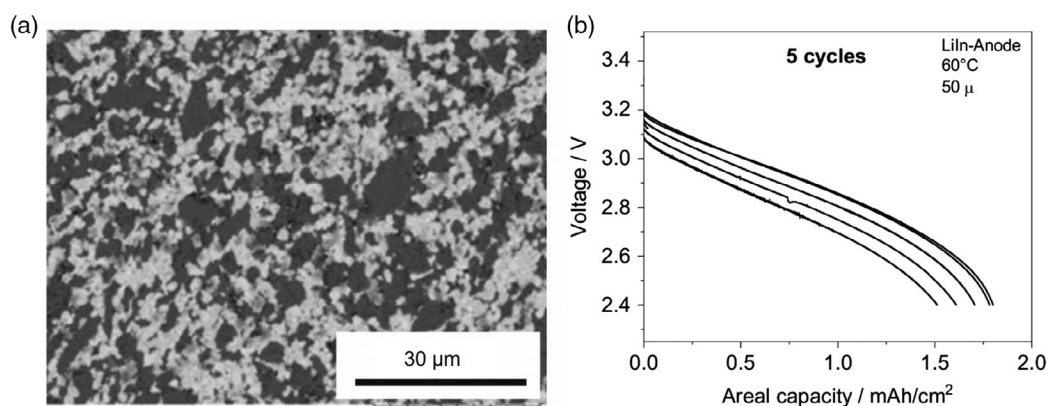


**Figure 2.** a) Cross-sectional image of composite cathode shows homogenous mixture of LLZ:Ta (bright) and LCO (dark gray) with a high relative density. b) Discharge curves of composite cathode in all-solid-state battery.



and low oxygen partial pressure like vacuum, Ar, or Ar/H<sub>2</sub>. The altering of stoichiometry is indicated by a color change in the sample. Furthermore, for these materials, change in lattice parameter might cause chemical expansion, which leads to internal stresses in the die, enhancing the risk crack formation during ejection.

To study this phenomena, GDC was sintered in a conventional FAST/SPS setup with graphite tools at 1400 °C, 4 min dwell time, and 50 MPa. A heating and cooling rate of 100 K min<sup>-1</sup> was applied. Vacuum or Ar-2.9% H<sub>2</sub> was used as the sintering atmosphere. In both cases, samples turned to a dark black color and were heavily cracked due to clamping effect and lack of atmosphere control inside the tool. To overcome this restriction, a pressure-less tool was designed, which enabled indirect heating of an isostatically pressed GDC sample (50 MPa, diameter 20 mm). As a specific tool design, a graphite ring was placed between the punches, forming a cavity in which the sample was positioned. To avoid direct contact to the graphite, the sample was placed on an Al<sub>2</sub>O<sub>3</sub> plate (thickness 3 mm). To enable gas transport to the sample, 4 mm holes were drilled through the graphite die and inserted ring. With this tool, a macroscopic stable sample could be sintered, but large microcracks were still observed by SEM. Therefore, an additional reoxidation step at 800 °C—as described in the literature<sup>[90]</sup> for conventional sintering of GDC—was introduced during the FAST/SPS sintering cycle for the first time. After sintering at 1400 °C, samples were cooled with 100 K min<sup>-1</sup> to 800 °C. Then, the chamber was evacuated for 4 min to 0.68 mbar and synthetic air (Ar-20% O<sub>2</sub>) was fed into the chamber. After another dwell time of 10 min, the sample was cooled down to room temperature. During the whole sintering cycle, oxygen partial pressure was measured by an oxygen sensor positioned at the gas outlet of the chamber (Figure 3a). Using this modified setup and processing conditions, cracking of the sample could be reliably avoided. Nevertheless, the color of the sintered sample was dark yellow (Figure 3b), still indicating a certain change in stoichiometry. XRD analysis (not shown here) confirmed that all samples maintained the initial cubic crystal structure. Our results reveal that a controlled atmosphere change is a possible option for sintering oxide ceramics in FAST/SPS devices,

but further studies regarding improved tool design are required to take full advantage of this option.

### 3.4. High-Temperature FAST/SPS of Refractory Materials and UHTCs

Sintering of high-temperature materials is quite challenging due to strong chemical bonds and low self-diffusion coefficients.<sup>[8]</sup> FAST/SPS is a quite promising method for densification of such materials due to superposition of pressure and—presupposed sufficient conductivity of the material—direct Joule heating. Current flow via the particle–particle contacts may destroy passivating oxide layers by vaporization or local melting. Furthermore, FAST/SPS is attractive for manufacturing of larger-sized samples with moderate shape complexities.<sup>[15]</sup> Here, two examples are given, which demonstrate the potential of FAST/SPS.

FAST/SPS of ZrB<sub>2</sub>: Gonzalez-Julian et al.<sup>[91]</sup> did a systematic study to improve sintering of ZrB<sub>2</sub> by FAST/SPS. ZrB<sub>2</sub> is a very promising material for high-temperature applications due to the extremely high melting temperature ( $T_m = 3246$  °C), high hardness, and chemical inertness. A low electrical resistance of 10 μΩ cm and good thermal conductivity ease densification of this material by FAST/SPS technology. The application of pressure-assisted sintering technologies like hot pressing is a standard for processing UHTCs. In the case of hot pressing, full densification can be achieved either at temperatures above 2000 °C in combination with moderate pressure in the range of 20–30 MPa or at a lowered temperature around 1800 °C in combination with a pressure above 800 MPa. Both attempts are quite challenging with respect to experimental equipment and tool design.

The focus of the study of Gonzalez-Julian et al. was to investigate the influence of current flow on densification. Therefore, three experimental setups were used. In setup I, current flow through the sample was avoided by applying BN discs between graphite punches and ZrB<sub>2</sub> powder. Setup II was the standard setup in FAST/SPS devices using graphite tool and punches. Graphite foil was applied to avoid chemical interaction between punch and ZrB<sub>2</sub> powder. Finally, in setup III, direct contact between graphite punch and sample enabled maximum current

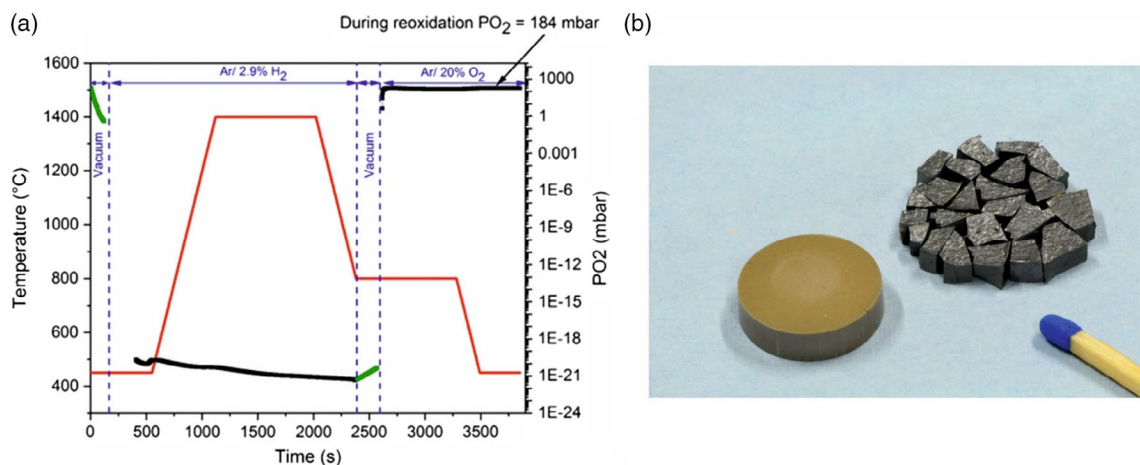


**Figure 3.** a) Controlled atmosphere change during a FAST/SPS cycle. b) GDC samples sintered in the conventional FAST/SPS setup (density of fragments 94%) and in a modified die with atmosphere change (density 93%).



flow via the sample. In all cases, FAST/SPS cycles were done with a heating rate of  $100 \text{ K min}^{-1}$ , a sintering temperature of  $1850^\circ\text{C}$ , a dwell time of 10 min, and a pressure of 50 MPa.

Up to  $1500^\circ\text{C}$ , densification rates were quite similar in all setups. Without current flow, a significant increase in densification rate already started at  $1500^\circ\text{C}$ . The samples achieved a density of  $5.83 \text{ g cm}^{-3}$  and a grain size around  $20 \mu\text{m}$ . In the case of current flow via the sample, onset of densification started and delayed at  $1650^\circ\text{C}$ . With increasing the current, density could be increased up to  $6.0 \text{ g cm}^{-3}$  and the amount of secondary phases was reduced. These effects were accompanied by a grain growth up to  $43 \mu\text{m}$ , which clearly hints on the influence of current flow on the sintering mechanisms. The improved sintering behavior in the case of current flow was explained by elimination/reduction of oxide layers ( $\text{B}_2\text{O}_3$  and  $\text{ZrO}_2$ ) on the particle surface, which is supposed to promote liquid phase sintering.

**FAST/SPS of ODS-W-11.4Cr-0.6Y:** Due to its high melting point and high thermal conductivity, tungsten is preferentially used as a plasma-facing armor material for the first wall of fusion reactors. Furthermore, tungsten is known for its low sputtering yield in contact with plasma particles, its low tritium retention, and its low erosion yield. Nevertheless, the stability of pure tungsten is limited in the case of loss-of-coolant accident (LOCA) in combination with air ingress in the case of leakage of the vacuum vessel. Related modelling predicts temperature increase up to  $1200^\circ\text{C}$  of tungsten armor due to nuclear decay heat. Elevated temperatures can last for up to several weeks in the worst case. In oxidation studies, it has been shown that the formation of thermodynamically less stable  $\text{WO}_3$  is coupled with strong sublimation, which can cause release of radioactive tungsten compounds to the environment. To overcome these restrictions, the development of so-called smart tungsten alloys was started recently at Institute of Energy and Climate Research (IEK-4: Plasma Physics). Up to now, W-11.4 wt% Cr-0.6 wt% Y was found to be the most promising alloy composition. Addition of Cr leads to the formation of a protecting  $\text{Cr}_2\text{O}_3$  layer in case of a LOCA. Y supports the formation of this oxide scale by finely distributed  $\text{YCrO}_3$  precipitations on grain boundaries, which helps to better control the Cr diffusion rate to the surface. Best protection is expected if this alloy is applied in bulk form with submicron grain sizes and  $\text{YCrO}_3$  finely dispersed on grain boundaries. For proof of concept, elemental W, Cr, and Y powders were mechanically alloyed in the required ratio. Details of powder preparation can be found in previous studies.<sup>[92,93]</sup> FAST/SPS was found to be the preferred method to produce

such kinds of microstructures. Full densification can be already achieved at temperatures significantly below the recrystallization temperature. Sintering at  $1460^\circ\text{C}$  in combination with high heating rates of  $200 \text{ K min}^{-1}$  resulted in grain sizes of  $0.23 \pm 0.03 \mu\text{m}$  (Figure 4a). Oxidation studies conducted at  $1000^\circ\text{C}$  showed a clearly improved oxidation resistance in the case of lowered grain sizes (Figure 4b).

### 3.5. Net Shaping in a FAST/SPS Device

One of the technical limitations of FAST/SPS is the shape of the sintered samples. Typically, cylindrical shapes, with thickness and diameter in the range of  $\text{mm cm}^{-1}$ , are consolidated. This is enough for fundamental investigation and optimization of the microstructure and properties, as well as for some applications where simple geometries are needed like sputter targets or brake elements. However, industry typically demands the production of dense components with more complex shapes. This is probably one of the main challenges in the FAST/SPS field to transfer the potential advantages of this technique—short sintering times, fine microstructure, lower temperature, etc.—to the market. Some approaches have been already conducted in this direction, such as the countering of the graphite tools, the use of multiple and independent punches, or using some sacrificial materials.<sup>[94–96]</sup> Certainly, these approaches are original and interesting, but they are relatively difficult to transfer to an industrial production. Probably, the most interesting approach with a high potential for large-scale industrial production is the use of a powder bed. This method was previously developed at the Belgian Ceramic Research Center and recently reported by Hocquet et al.<sup>[97]</sup> and by Manière et al.<sup>[98]</sup>

We applied a similar approach to densify ceramics with near net shapes. In this case, we use a MAX phase as reference material, in particular,  $\text{Ti}_2\text{AlC}$ , due to the high potential of this composition. The green near-net shape—a gear wheel—was processed by injection molding, and the experimental procedure is described in previous studies.<sup>[99]</sup> Regarding the powder bed, carbon powder was used due to high thermal conductivity and stability as well as low sinterability at the desired temperature. In this case, no interfacial materials were used between the sample and the powder bed. Nevertheless, if a reaction is expected, an interfacial material such as BN or graphite foils might be used. The gear wheel was placed into the carbon bed (Figure 5a), and the whole system was located between the punches as in a conventional FAST/SPS procedure. The sintering parameters were a

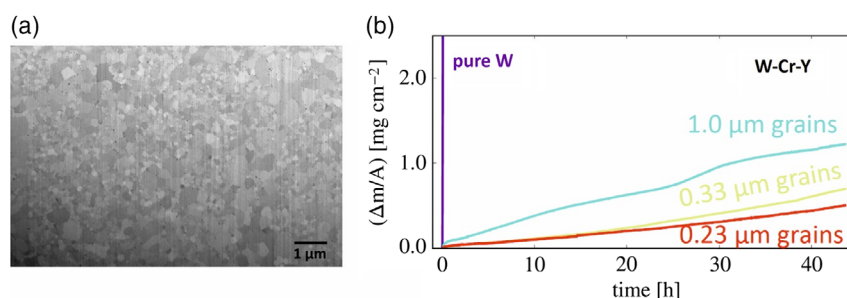


**Figure 4.** a) Microstructure of W-11.6Cr-0.6Y alloy sintered by FAST/SPS at  $1460^\circ\text{C}$  (50 MPa, heating rate  $200^\circ\text{C min}^{-1}$ , dwell time 0 min). b) Oxidation rates of W-11.6Cr-0.6Y alloy depending on the grain size. Published under Creative Commons CC-BY license in the study by Klein et al.<sup>[93]</sup>

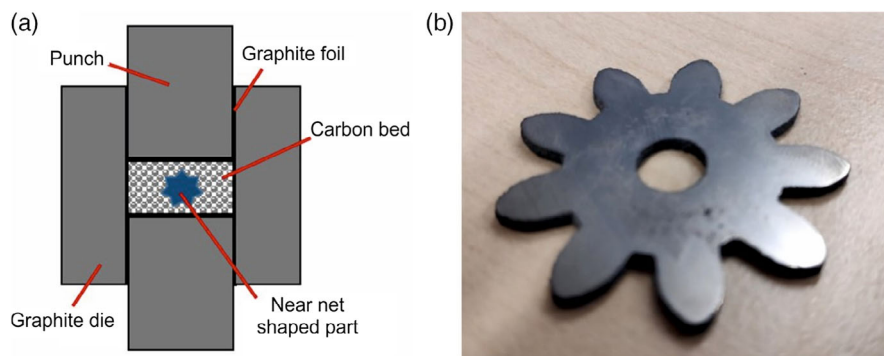


**Figure 5.** a) Scheme of the carbon powder bed in FAST/SPS and b) photograph of the sintered  $\text{Ti}_2\text{AlC}$  gear wheel.

heating rate of  $100 \text{ K min}^{-1}$ , maximal temperature of  $1350^\circ\text{C}$ , dwell time of 20 min, 50 MPa of uniaxial pressure during the whole thermal treatment, and vacuum atmosphere. The sample presented a relative density of 98.2% (Figure 5b), whereas only 89.6% was achieved by pressureless sintering at the same maximal temperature. As mentioned, uniaxial pressure was used during the thermal treatment, but the sample was sintered in pseudoisostatic conditions due to its embedding in carbon powder. The mechanical load is axially transferred to the sample but also radial forces are expected. The pseudoisostatic contribution has to be certainly investigated in more detail, and modeling is one of the best approaches for its understanding and quantification. Furthermore, in addition to the sintering of complex shapes, carbon bed approach exhibits a high potential because several samples can be consolidated in just one thermal cycle.

### 3.6. Scaling up FAST/SPS Technology for Effective Sintering of Oxide Ceramics

Further scaling up and industrialization of FAST/SPS technologies require critical analysis of energy consumption and ideas to reduce temperature gradients, which is up to now rarely discussed in literature.<sup>[15,70,71,100]</sup> A complete energy balance including energy consumed by the water-cooling system is usually not discussed. Therefore, a preliminary investigation of energy consumption and temperature gradients was conducted at IEK-1 within a FAST/SPS setup with a die of 17 mm in diameter.<sup>[11]</sup> The tool was mounted in the HP-D5 device. The active power consumed by HP-D5 device was recorded by an internal data logger. The temperature distribution within the setup was calculated by FEM. Both experiments and modeling were conducted for conductive 316L metallic powder and for nonconductive 8YSZ ceramic powder. It was found that at properly designed thermal insulation of the die the power required for sintering can be reduced by a factor of 2. If additionally the graphite spacer was replaced by a CFRC spacer with a lesser thermal conductivity, the power consumption was reduced by a factor of 3 for 316L powder and 5 for 8YSZ powder. Further measurement of power consumed by the water-cooling aggregate has shown that  $\approx 30\%$  of total energy demand is used by this device. For measurement of total energy consumption, the external data logger PEL 103 (Chauvin Arnoux, France) was applied. Numerical simulation

has revealed that thermal insulation decreases temperature gradients. The decrease is especially pronounced for sintering of nonconductive 8YSZ samples with a large diameter.

This approach was extended to the investigation of energy demand in the larger H-HP-D25 device. Active power and related energy consumption during the sintering of  $\text{Y}_2\text{O}_3$  discs with a diameter of 100 mm were measured in a setup shown in Figure 6. In addition, the power and energy consumed by the water-cooling device were recorded. Again, the external data logger PEL 103 was used.

The reduction in power and energy demands with the application of CFRC spacer was noticed during our experiments in the smaller HP-D5 device. This was explained by the low thermal conductivity of CFRC material. Therefore, we first assumed that the application of CFRC plates with a thickness of 10 mm in the setup developed for sintering in H-HP-D25 SD/FL/MoSi device should result in a similar effect. To clarify the influence of CFRC plate's location on energy demand, sintering with three different CFRC positions was conducted. These positions are shown in Table 1. The sintering cycle was the same in all experiments. This cycle included heating with  $25 \text{ K min}^{-1}$  to a temperature of  $1400^\circ\text{C}$ , following holding at this temperature for 30 min, and rapid cooling with cooling aggregate in operation. A pressure of 30 MPa was applied before heating. The pressure was released at dwell and in all cycles, thermal insulation of external die wall was applied. Nevertheless, only a relatively slow heating rate of maximum  $25 \text{ K min}^{-1}$  was possible in the large setup.

In contrast to our expectation only a moderate influence of the position of CFRC spacer on heating energy was observed. Moreover, cooling energy was fully unaffected by the location of CFRC plates. In contrast, the energy consumed by the cooling device is  $\approx 30\%$  of total energy demand. This number is in good correlation with our data obtained in similar experiments with HP-D5.

### 3.7. From FAST/SPS to FS

A promising alternative to FAST/SPS is FS, which is based on forcing a current flow through the sample by applying an enhanced electric field at moderate furnace temperatures, where rapid densification in less than 5 s can be achieved.<sup>[51]</sup> Due to the fact that the electric power is almost completely dissipated by the sample, it is expected to be very energy efficient and economic.

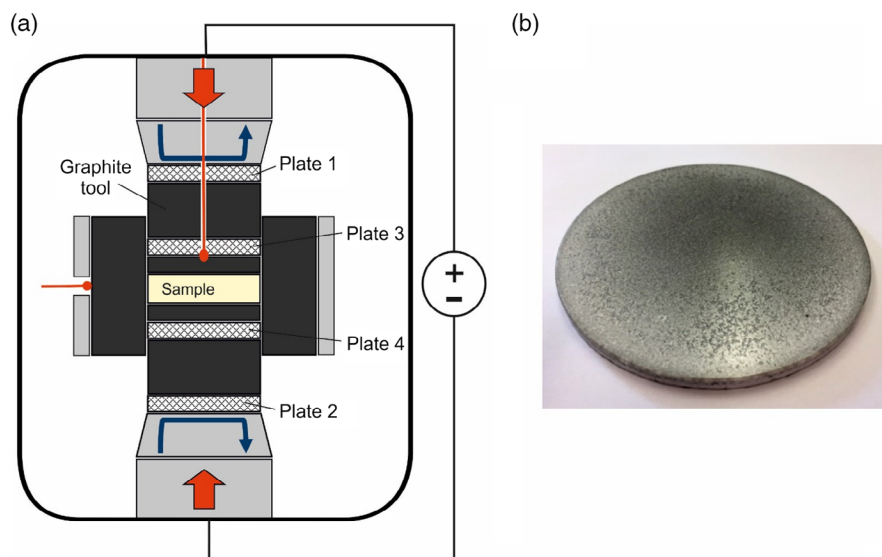


**Figure 6.** a) Experimental setup used for sintering of  $\text{Y}_2\text{O}_3$  discs in H-HP-D25 SD/FL/MoSi device. b)  $\text{Y}_2\text{O}_3$  disc with diameter 100 mm.

**Table 1.** Energy demand of the H-HP-D 25 SD/FL/MoSi device (heating energy) and cooling device in the case of sintering  $\text{Y}_2\text{O}_3$  discs with diameter 100 mm.

Case of study	Setup I	Setup II	Setup III
Plates 1 and 2	CFRC	Graphite	CFRC
Plates 3 and 4	CFRC	CFRC	Graphite
Heating energy [kWh]	38.48	42.30	42.99
Cooling energy [kWh]	17.71	17.62	17.54
Total Energy [kWh]	56.19	59.62	60.53

The experimental setup shown in **Figure 7a** enables to conduct FS cycles in our H-HP-D25 SD/FL/MoSi device. First experiments with 8YSZ powders were done pointing out the main

challenge of FS, especially if aiming at upscaling the technology. For conducting the FS cycle, FS parameters from the literature were considered.<sup>[101]</sup> 8YSZ powder was filled in a 45 mm graphite tool. To force the current through the powder bed, an electrically isolating BN inlay was inserted in the graphite die (Figure 7a). Then an electric field of  $150 \text{ V cm}^{-1}$  was applied, and the temperature was raised at  $10^\circ\text{C}$  from  $250^\circ\text{C}$  to the flash temperature. The onset of flash occurred at  $700^\circ\text{C}$ . In the given conditions, the flash event resulted in an only partial densification of the sample due to hot spot formation (Figure 7b). Hot spot formation means that current channels through localized paths in the sample, which is often accompanied by local melting or fracture of the sample. Density gradients in the powder compact and imperfect electrical contacts at the abutting faces are discussed as main reasons of hot spot formation.

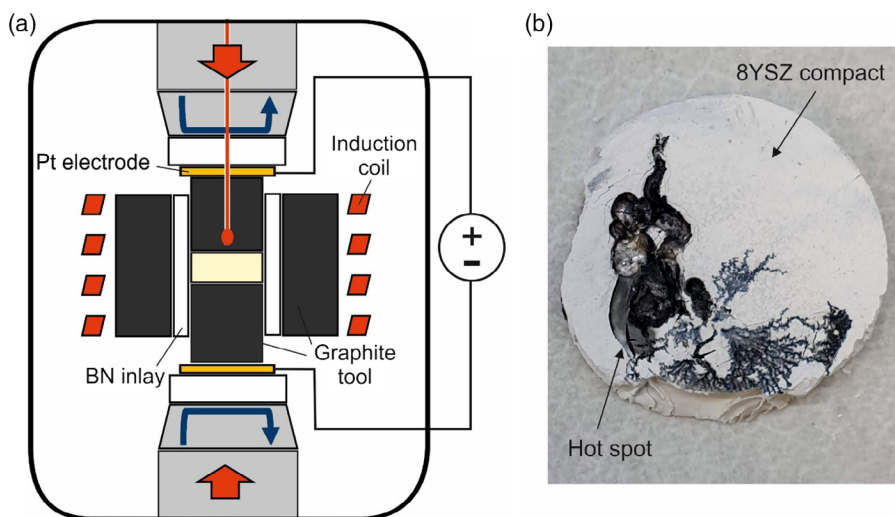


**Figure 7.** a) Experimental setup for FS in Hybrid FAST/SPS device H-HP-D25 SD/FL/MoSi graphite tool with BN inlay, induction heating. b) Hot spot formation if conducting a flash cycle in isothermal mode (sample diameter 45 mm).

To overcome the hot spot formation, the following strategy will be applied in our future works. Recent experiments on dog bone-shaped GDC samples revealed that FS with a linear increase in the current at a controlled rate to a maximum current density is the key for reliably controlling FS.<sup>[102–104]</sup> In this novel FS mode, the current was controlled from the beginning of the sintering cycle and increased at a constant rate and constant furnace temperature until the maximum current density was achieved. To determine the optimum sintering parameters for current rate-controlled FS, a sintering map based on constant heating rate experiments and isothermal FS experiments will be generated. The sintering map and related microstructure investigations help to better understand the relationship between current density and densification of the sample. In addition to parameters directly related to the flash event, processing parameters like density of the compact, external pressure, contact between electrodes and sample, and the application of thermal insulation will be systematically varied to identify optimum conditions for reproducible FS. Finally, energy consumption of FS will be measured to estimate the potential of FS compared with other sintering technologies in an objective way.

## 4. Conclusions and Outlook

The Institute of Energy and Climate Research (IEK-1: Materials Synthesis and Processing) of Forschungszentrum Jülich GmbH offers a unique platform for investigating field-assisted sintering technologies. For example, one of our devices is equipped with an additional induction or resistance heater, which enables operation in the hybrid FAST/SPS mode. Furthermore, a separate 1000 V power source even allows to conduct FS cycles, which is quite rare so far in such devices. Field- and pressure-assisted sintering technologies are attractive for the densification of ceramic or metal powders, which are difficult to sinter due to the low sintering activity or limited stability. Furthermore, direct heat transfer and—in the case of sufficient conductivity of the powder—Joule heating of the sample enable high heating rates, which are helpful to reduce grain growth. Mesoscale and macroscopic modeling is required to control this dynamic process. Sintering parameters such as uniaxial viscosities, sintering stresses, and viscous Poisson's ratio are necessary input parameters. They can be experimentally measured with our custom-made instrumented sinter forging in electric field.<sup>[61,62]</sup>

Currently, several challenges exist for taking full advantage of FAST/SPS and FS technologies. Most of these challenges are addressed in this article, and an overview of our current activities is given. Important topics are cold sintering of nanoscaled powders with water as the additive, high-pressure sintering of battery materials at moderate temperatures, sintering of oxides which are prone to chemical expansion, and sintering of refractory materials. Furthermore, our ongoing work deals with net-shape manufacturing, scaling up of technology, and first attempts of FS in a FAST/SPS apparatus. Further, systematic studies will enable to find solutions to the mentioned challenges. To get more detailed information on the different work topics, we refer to the related publications.

## Acknowledgements

Parts of this study were funded by the Deutsche Forschungsgemeinschaft (DFG) in the framework of the priority program SPP1959 (funding reference BR3418/1-1 and GU993/9-1). The work on battery materials was funded by Bundesministerium für Bildung und Forschung (BMBF) in the framework of the EvaBATT project (funding reference 13XP0134A). We are very grateful for the funding received.

## Conflict of Interest

The authors declare no conflict of interest.

## Keywords

electric current-assisted sintering, field-assisted sintering technique/spark plasma sintering, flash sintering, materials for energy applications

Received: January 13, 2020

Revised: February 6, 2020

Published online: April 13, 2020

- [1] O. Guillon, C. Elsässer, O. Gutfleisch, J. Janek, S. Korte-Kerzel, D. Raabe, C. A. Volkert, *Mater. Today* **2018**, 21, 527.
- [2] R. Orrù, R. Licheri, A. M. Locci, A. Cinotti, G. Cao, *Mater. Sci. Eng. R.* **2009**, 63, 127.
- [3] S. Grasso, Y. Sakka, G. Maizza, *Sci. Technol. Adv. Mater.* **2009**, 10, 053001.
- [4] Z. A. Munir, D. V. Quach, M. Ohyanagi, *J. Am. Ceram. Soc.* **2011**, 94, 1.
- [5] J. E. Garay, *Annu. Rev. Mater. Res.* **2010**, 40, 445.
- [6] *Spark Plasma Sintering* (Eds: G. Cao, C. Estournes, J. Garay, R. Orru), Elsevier, Amsterdam **2019**.
- [7] *Field-Assisted Sintering: Science and Applications* (Eds: E. A. Olevsky, D. V. Dudina), Springer, Cham **2018**.
- [8] *Spark Plasma Sintering of Materials* (Ed: P. Chavalier), Springer, Cham **2019**.
- [9] Z. A. Munir, U. Anselmi-Tamburini, M. Ohyanagi, *J. Mater. Sci.* **2006**, 41, 763.
- [10] O. Guillon, J. Gonzalez-Julian, B. Dargatz, T. Kessel, G. Schierning, J. Räthel, M. Hermann, *Adv. Eng. Mater.* **2014**, 16, 1.
- [11] A. M. Laptev, M. Bram, K. Vanmeensel, J. Gonzalez-Julian, O. Guillon, *J. Mater. Proc. Technol.* **2018**, 262, 326.
- [12] <https://www.mersen.com/products/graphite-specialties/isostatic-graphite-and-extruded-graphite/sintering> (accessed: January 06, 2020).
- [13] K. Vanmeensel, A. Laptev, J. Hennicke, J. Vleugels, O. Van der Biest, *Acta Mater.* **2005**, 53, 4379.
- [14] M. Beekman, M. Baitinger, H. Borrmann, W. Schnelle, K. Meier, G. S. Nolas, Y. Grin, *J. Am. Chem. Soc.* **2009**, 131, 9642.
- [15] J. Hennicke, T. Kessel, S. Rivera Monte, *cf/Ber. DKG* **2018**, 95, E27.
- [16] R. Kali, A. Mukhopadhyay, *J. Power Sources* **2014**, 247, 920.
- [17] S. Ramakumar, C. Devianapoorani, L. Dhiyya, L. S. Shankar, R. Murugan, *Prog. Mater. Sci.* **2017**, 88, 325.
- [18] G. Lee, E. A. Olevsky, C. Manière, A. Maximenko, O. Izhevskov, C. Back, J. McKittrick, *Acta Mater.* **2018**, 144, 524.
- [19] K. Morita, B.-N. Kim, H. Yoshida, K. Hiraga, Y. Sakka, *J. Am. Ceram. Soc.* **2015**, 98, 378.
- [20] U. Anselmi-Tamburini, J. N. Woolman, Z. A. Munir, *Adv. Funct. Mater.* **2007**, 17, 3267.
- [21] E. Colombini, R. Rosa, L. Trombi, *Mater. Chem. Phys.* **2018**, 210, 78.

- [22] J. P. Siebert, C. M. Hamm, C. S. Birkel, *Appl. Phys. Rev.* **2019**, 6, 5121442.
- [23] A. Bisht, M. Srivastava, R. M. Kumar, I. Lahiri, D. Lahiri, *Mater. Sci. Eng. A* **2017**, 695, 20.
- [24] Y. Cheng, Z. Cui, L. Cheng, D. Gong, W. Wang, *Adv. Powder Technol.* **2017**, 28, 1129.
- [25] M. Mondet, E. Barraud, J. Lemmonier, N. Allain, T. Grosdidier, *Acta Mater.* **2016**, 119, 55.
- [26] L. M. Kang, C. Yang, *Adv. Eng. Mater.* **2019**, 21, 1801359.
- [27] C. Yang, L. M. Kang, X. X. Li, W. W. Zhang, D. T. Zhang, Z. Q. Fu, Y. Y. Li, L. C. Zhang, E. J. Lavernia, *Acta Mater.* **2017**, 132, 491.
- [28] Y. Y. Li, L. M. Zhou, C. Yang, Y. H. Li, L. J. Li, *Mater. Sci. Eng. A* **2013**, 560, 857.
- [29] Y. H. Li, C. Yang, F. Wang, H. D. Zhao, S. G. Qu, X. Q. Li, W. W. Zhang, Y. Y. Li, *Mater. Design* **2015**, 85, 7.
- [30] Z. H. Zhang, Z.-F. Liu, J. F. Lu, X. B. Shen, F.-C. Wang, Y. D. Wang, *Scr. Mater.* **2014**, 81, 56.
- [31] J. Gonzalez-Julian, O. Guillon, *J. Am. Ceram. Soc.* **2015**, 98, 2018.
- [32] C. Manière, E. A. Olevsky, *Scr. Mater.* **2017**, 141, 62.
- [33] C. Yang, M. D. Zhu, X. Luo, L. H. Liu, W. W. Zhang, Y. Long, Z. Y. Xiao, Z. Q. Fu, L. C. Zheng, E. J. Lavernia, *Scr. Mater.* **2017**, 139, 96.
- [34] X. X. Li, C. Yang, T. Chen, Z. Q. Fu, Y. Y. Li, O. M. Ivasishin, E. J. Lavernia, *Scr. Mater.* **2018**, 151, 47.
- [35] J. Zhou, K. Hirao, Y. Yamanchi, S. Kanzaki, *J. Eur. Ceram. Soc.* **2004**, 24, 3465.
- [36] C. Yang, Y. J. Zhao, Z. Wang, S. G. Qu, X. Q. Li, W. W. Zhang, L. C. Zhang, *Metall. Mater. Trans. A* **2019**, 50, 856.
- [37] C. Yang, J. A. Lin, Y. F. Ding, W. W. Zhang, Y. Y. Li, Z. Q. Fu, F. Chen, E. J. Lavernia, *J. Mater. Sci.* **2016**, 51, 10608.
- [38] D. V. Dudina, B. B. Bokhonov, E. A. Olevsky, *Materials* **2019**, 12, 541.
- [39] S. Grasso, T. Saunders, H. Porwal, O. Cedillos-Barraza, D. D. Jayaseelan, W. E. Lee, M. J. Reece, *J. Am. Ceram. Soc.* **2014**, 97, 2405.
- [40] S. Grasso, T. Saunders, H. Porwal, B. Milson, A. Tudball, M. J. Reece, *J. Am. Ceram. Soc.* **2016**, 99, 1534.
- [41] E. Castle, R. Sheridan, W. Zhou, S. Grasso, A. Walton, M. J. Reece, *Sci. Rep.* **2017**, 7, 11134.
- [42] M. Yu, T. Saunders, S. Grasso, A. Mahajan, H. Zhang, M. J. Reece, *Scr. Mater.* **2018**, 146, 241.
- [43] G. Manière, G. Lee, E. A. Olevsky, *Sci. Rep.* **2017**, 7, 15071.
- [44] A. Fais, *J. Mater. Proc. Technol.* **2010**, 210, 2223.
- [45] L. Leich, A. Röttger, M. Krengel, W. Theisen, *J. Sustainable Metall.* **2019**, 5, 107.
- [46] M. A. Lagos, I. Agote, T. Schubert, T. Weissgaerber, J. M. Gallardo, J. M. Montes, L. Prakash, C. Andreouli, V. Oikonomou, D. Lopez, J. A. Calero, *Int. J. Refract. Met. Hard Mater.* **2017**, 66, 88.
- [47] B. Niu, F. Zhang, J. Zhang, W. Ji, W. Wang, Z. Fu, *Scr. Mater.* **2016**, 116, 127.
- [48] D. Demirskyi, O. Vasykiv, *J. Alloys Compd.* **2017**, 691, 466.
- [49] E. Zapata-Solvas, D. Gomez-Garcia, A. Dominguez-Rodriguez, R. I. Todd, *Sci. Rep.* **2015**, 5, 8513.
- [50] O. Vasykiv, H. Borodianska, Y. Sakka, D. Demirskyi, *Scr. Mater.* **2016**, 121, 32.
- [51] M. Cologna, B. Rashkova, R. Raj, *J. Am. Ceram. Soc.* **2010**, 93, 3556.
- [52] M. Yu, S. Grasso, R. Mckinnon, T. Saunders, M. J. Reece, *Adv. Appl. Ceram.* **2017**, 116, 24.
- [53] C. E. J. Dancer, *Mater. Res. Express.* **2016**, 3, 102001.
- [54] <https://www.lucideon.com/materials-technologies/flash-sintering> (accessed: December 20, 2019).
- [55] R. I. Todd, E. Zapata-Solvas, R. S. Bonilla, T. Sneddon, P. R. Wilshaw, *J. Eur. Ceram. Soc.* **2015**, 35, 1865.
- [56] Y. Dong, I. W. Chen, *J. Am. Ceram. Soc.* **2015**, 98, 3624.
- [57] R. Chaim, *Materials* **2016**, 9, 19.
- [58] J. Narayan, *Scr. Mater.* **2013**, 69, 107.
- [59] W. Ji, B. Parker, S. Falco, J. Y. Zhang, Z. Y. Fu, R. I. Todd, *J. Eur. Ceram. Soc.* **2017**, 37, 2547.
- [60] C. Cao, R. Mücke, O. Guillon, *Scr. Mater.* **2020**, 182, 77.
- [61] C. Cao, R. Mücke, F. Wakai, O. Guillon, *Scr. Mater.* **2020**, 178, 240.
- [62] J. S. C. Francis, M. Cologna, R. Raj, *J. Eur. Ceram. Soc.* **2012**, 32, 3129.
- [63] M. Jongmanns, R. Raj, D. E. Wolf, *New J. Phys.* **2018**, 20, 93013.
- [64] M. Biesuz, V. M. Sglavo, *J. Eur. Ceram. Soc.* **2019**, 39, 115.
- [65] S. Schwarz, O. Guillon, *J. Eur. Ceram. Soc.* **2013**, 33, 637.
- [66] <https://www.bohler.de/de/products/w360/> (accessed: January 06, 2020).
- [67] <https://www.plansee.com/en/materials/molybdenum.html> (accessed: January 06, 2020).
- [68] J. Pereira da Silva, M. Bram, A. M. Laptev, J. Gonzalez-Julian, Q. Ma, F. Tietz, O. Guillon, *J. Eur. Ceram. Soc.* **2019**, 39, 2697.
- [69] A. M. Laptev, H. Zheng, M. Bram, M. Finsterbusch, O. Guillon, *Mater. Lett.* **2019**, 247, 155.
- [70] A. Zavaliangos, J. Zhang, M. Krammer, J. R. Groza, *Mater. Sci. Eng. A* **2004**, 379, 218.
- [71] K. Vanmeensel, A. M. Laptev, J. Hennicke, J. Vleugels, O. Van der Biest, *Acta Mater.* **2007**, 55, 1801.
- [72] T. Herisson de Beauvoir, A. Sangregorio, I. Cornu, C. Elissalde, M. Josse, *J. Mater. Chem. C* **2018**, 6, 2229.
- [73] M. Biesuz, G. Taveri, A. I. Duff, E. Olevsky, D. Zhu, C. Hu, S. Grasso, *Adv. Appl. Ceram.* **2020**, 119, 75.
- [74] J. Guo, H. Guo, A. L. Baker, M. T. Lanagan, E. R. Kupp, G. L. Messing, C. A. Randall, *Angew. Chem. Int. Ed.* **2016**, 55, 11457.
- [75] H. Guo, A. Baker, J. Guo, C. A. Randall, *J. Am. Ceram. Soc.* **2016**, 99, 3489.
- [76] B. Dargatz, J. Gonzalez-Julian, M. Bram, P. Jakes, A. Besmehn, L. Schade, R. Röder, C. Ronning, O. Guillon, *J. Eur. Ceram. Soc.* **2016**, 36, 1207.
- [77] J. Gonzalez-Julian, K. Neuhaus, M. Bernemann, J. Pereira da Silva, A. M. Laptev, M. Bram, O. Guillon, *Acta Mater.* **2018**, 144, 116.
- [78] S. Schwarz, A. M. Thron, J. Rufner, K. Van Benthem, O. Guillon, *J. Am. Ceram. Soc.* **2012**, 95, 2451.
- [79] B. Dargatz, J. Gonzalez-Julian, M. Bram, Y. Shinoda, F. Wakai, O. Guillon, *J. Eur. Ceram. Soc.* **2016**, 36, 1221.
- [80] Y. Ren, T. Liu, Y. Shen, Y. Lin, C. W. Nan, *J. Materiomics* **2016**, 2, 256.
- [81] L. Miara, A. Windmüller, C. L. Tsai, W. D. Richards, Q. Ma, S. Uhlenbruck, O. Guillon, G. Ceder, *ACS Appl. Mater. Interfaces* **2016**, 8, 26842.
- [82] K. H. Kim, Y. Iriyama, K. Yamamoto, S. Kumazaki, T. Asaka, K. Tanabe, C. A. J. Fisher, T. Hirayama, R. Murugan, Z. Ogumi, *J. Power Sources* **2011**, 196, 764.
- [83] F. Han, J. Yue, C. Chen, N. Zhao, X. Fan, Z. Ma, T. Gao, F. Wang, X. Guo, C. Wang, *Joule* **2018**, 2, 497.
- [84] K. Park, B. C. Yu, J. W. Jung, Y. Li, W. Zhou, H. Gao, S. Son, J. B. Goodenough, *Chem. Mater.* **2016**, 28, 8051.
- [85] C. L. Tsai, Q. Ma, C. Dellen, S. Lobe, F. Vondahlen, A. Windmüller, D. Grüner, H. Zheng, S. Uhlenbruck, M. Finsterbusch, F. Tietz, D. Fattakhova-Rohlfing, H. P. Buchkremer, O. Guillon, *Sustainable Energy Fuels* **2019**, 3, 280.
- [86] L. Cheng, J. S. Park, H. Hou, V. Zorba, G. Chen, T. Richardson, J. Cabana, R. Russo, M. Doeff, *J. Mater. Chem. A* **2014**, 2, 172.
- [87] E. Antolini, M. Feretti, *J. Solid State Chem.* **1995**, 117, 1.
- [88] Y. Li, X. Chen, A. Dolocan, Z. Cui, S. Xin, L. Xue, H. Xu, K. Park, J. B. Goodenough, *J. Am. Ceram. Soc.* **2018**, 140, 6448.
- [89] M. Finsterbusch, T. Danner, C. L. Tsai, S. Uhlenbruck, A. Latz, O. Guillon, *ACS Appl. Mater. Interfaces* **2018**, 10, 22329.
- [90] D. Ni, J. Glasscock, A. Pons, W. Zhang, A. Prasad, S. Sanna, N. Pryds, V. Esposito, *J. Electrochem. Soc.* **2014**, 161, 3072.
- [91] J. Gonzalez-Julian, K. Jähnert, K. Speer, L. Liu, J. Räthel, M. Knapp, H. Ehrenberg, M. Bram, O. Guillon, *J. Am. Ceram. Soc.* **2016**, 99, 35.

- [92] A. Litnovsky, T. Wegener, F. Klein, Ch Linsmeier, M. Rasinski, A. Kreter, X. Tan, J. Schmitz, J. W. Coenen, Y. Mao, J. Gonzalez-Julian, M. Bram, *Phys. Scr.* **2017**, T170, 014012.
- [93] F. Klein, T. Wegener, A. Litnovsky, M. Rasinski, X. Y. Tan, J. Gonzalez-Julian, J. Schmitz, M. Bram, J. W. Coenen, Ch Linsmeier, *Nucl. Mater. Energy* **2018**, 15, 226.
- [94] T. Voisin, J. Monchoux, L. Durand, N. Karnatak, M. Thomas, A. Couret, *Adv. Eng. Mater.* **2015**, 17, 1408.
- [95] C. Maniere, L. Dunand, A. Weibel, G. Chevallier, C. Estournes, *Scr. Mater.* **2016**, 124, 126.
- [96] C. Maniere, E. Torresani, E. A. Olevsky, *Materials* **2019**, 12, 1.
- [97] S. Hocquet, V. Dupont, F. Chambier, F. Ludewig, N. Vandewalle, *J. Eur. Ceram. Soc.* **2019**, <https://doi.org/10.1016/j.jeurceramsoc.2019.10.038>.
- [98] C. Manière, E. Nigito, L. Durand, A. Weibel, Y. Beynet, C. Estournes, *Powder Technol.* **2017**, 320, 340.
- [99] J. Gonzalez-Julian, L. Classen, M. Bram, R. Vassen, O. Guillon, *J. Am. Ceram. Soc.* **2016**, 99, 3210.
- [100] D. Giuntini, E. A. Olevsky, C. Garcia-Cardona, A. L. Maximenko, C. D. Haines, D. G. Martin, D. Kapoor, *Materials* **2013**, 6, 2612.
- [101] M. Cologna, A. L. G. Prette, R. Raj, *J. Am. Ceram. Soc.* **2011**, 94, 316.
- [102] P. Kumar, D. Yadav, J. M. Lebrun, R. Raj, *J. Am. Ceram. Soc.* **2019**, 102, 823.
- [103] H. Charalambous, S. K. Jha, K. H. Christian, R. T. Lay, T. Tsakalakos, *J. Eur. Ceram. Soc.* **2018**, 38, 3689.
- [104] T. P. Mishra, R. R. Ingraci Neto, R. Raj, O. Guillon, M. Bram, *Acta Mat.* **2020**, <https://doi.org/10.1016/j.actamat.2020.02.036>.